NASA Technical Paper 3610

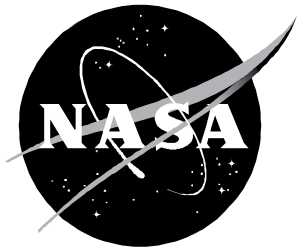

Calibration of NASA Turbulent Air Motion Measurement System

John D. W. Barrick, John A. Ritter, Catherine E. Watson, Mark W. Wynkoop, John K. Quinn, and Daniel R. Norfolk
Langley Research Center • Hampton, Virginia

National Aeronautics and Space Administration
Langley Research Center • Hampton, Virginia 23681-0001

December 1996

Acknowledgments

This effort would not have been possible without the support and assistance of the staff of the Wallops Flight Facility and the flight crew of the Electra airplane. Their cooperation and effort in executing precise flight maneuvers and ground calibration procedures ensured the quality and overall integrity of the TAMMS calibration. We would also like to thank Riley S. Bull, Prentiss J. Moore, and Charles S. West of Wallops for their cooperation and efforts in the instrumentation of the tower used for correlative ground measurements.

Available electronically at the following URL address: http://techreports.larc.nasa.gov/ltrs/ltrs.html

Printed copies available from the following:

NASA Center for AeroSpace Information
800 Elkridge Landing Road
Linthicum Heights, MD 21090-2934
(301) 621-0390

National Technical Information Service (NTIS)
5285 Port Royal Road
Springfield, VA 22161-2171
(703) 487-4650

Contents

Symbols

C_L	lift coefficient
c	atmospheric trace species
c'	fluctuation of trace species from mean value
D	fuselage diameter, m
e	partial vapor pressure, hPa
f	function
GOES	Geostationary Operational Environment Satellite
INS	inertial navigation system
L	lift of airplane, which is equivalent to weight for level flight
M	Mach number
M_l	local Mach number
p	free-stream static pressure, hPa
Δp	static pressure position error, hPa
p'	local static pressure, hPa
$p_{s,\text{ref}}$	static pressure interpolated to airplane sensor height by using tower measurements, hPa
p_t	total pressure, hPa
q_c	dynamic pressure, hPa
q_c'	local dynamic pressure, hPa
R	gas constant
r	recovery factor for sensor
S	wing area, m^2
TAMMS	turbulent air motion measurement system
T_m	measured air temperature, °C
T_r	recovery temperature, °C
T_s	corrected static air temperature, °C
T_s'	static air temperature corrected for Mach number only, °C
$T_{s,\text{ref}}$	static air temperature interpolated to airplane sensor height by using tower measurements, °C
T_t	total air temperature, °C
T_x	air temperature error due to heat-transfer effects, °C
T_1	air temperature measured at 76.2-m tower level, °C
U_a	true airspeed, $m\text{-}s^{-1}$
u	east-west horizontal wind velocity component, $m\text{-}s^{-1}$
u_p	east-west airplane velocity component with respect to Earth, $m\text{-}s^{-1}$
v	north-south horizontal wind velocity component, $m\text{-}s^{-1}$
v_a	air velocity with respect to airplane, $m\text{-}s^{-1}$
v_p	north-south airplane velocity component with respect to Earth, $m\text{-}s^{-1}$
w	vertical wind velocity component, $m\text{-}s^{-1}$

w'	fluctuation of vertical wind component from mean value, m-s^{-1}
w_p	vertical airplane velocity component with respect to Earth, m-s^{-1}
x	distance of static port in front of airplane nose, m
z	height of airplane static port, m
Δz	distance of airplane static port below 91.5-m tower level, m
α	angle of attack, deg
β	angle of sideslip, deg
γ	ratio of specific heats
γ_o	ratio of specific heat for dry air, 1.4028
η	air temperature probe recovery correction
θ	pitch angle, deg
ψ	airplane heading, deg

Abstract

A turbulent air motion measurement system (TAMMS) was integrated onboard the Lockheed 188 Electra airplane (designated NASA 429) based at the Wallops Flight Facility in support of the NASA role in global tropospheric research. The system provides air motion and turbulence measurements from an airborne platform which is capable of sampling tropospheric and planetary boundary-layer conditions. TAMMS consists of a gust probe with free-rotating vanes mounted on a 3.7-m epoxy-graphite composite nose boom, a high-resolution inertial navigation system (INS), and data acquisition system. A variation of the tower flyby method augmented with radar tracking was implemented for the calibration of static pressure position error and air temperature probe. Additional flight calibration maneuvers were performed remote from the tower in homogeneous atmospheric conditions. System hardware and instrumentation are described and the calibration procedures discussed. Calibration and flight results are presented to illustrate the overall ability of the system to determine the three-component ambient wind fields during straight and level flight conditions.

1. Introduction

Airborne air motion measurement systems have progressed from the research and development stage (Lenschow 1972; Meissner 1976; Lenschow et al. 1978) to a resource that is appropriate for a variety of applications in the atmospheric sciences. The accurate determination of the ambient three-component wind field from a moving platform has proven to be a very challenging problem because a relatively small result must be determined from the difference between two large values. The relative motion of an aircraft with respect to the Earth must be subtracted from the velocity of the air with respect to the aircraft in order to obtain the ambient wind field. As a result, both sets of these relative velocity measurements require a high level of accuracy to meet the measurement requirements for modern applications. Advances in the accuracy of inertial sensors and data analysis are responsible for the development of these systems and for their expanding utility (Axford 1968; Telford and Wagner 1974; Telford, Wagner, and Vaziri 1977; LeMone and Pennell, 1980; Frost, Paige, and Nelius 1991).

Presently, air motion systems operate on many types of research aircraft that encompass a broad spectrum of flight conditions. These systems basically follow the same approach by measuring relative ground motion via an inertial navigation system (INS) but differ slightly in their measurement approach for relative air motion. Most systems have used either a gust probe (a pitot-static tube with flow directional vanes) affixed to a nose boom (Lenschow 1972; Gilmer, McGavin, and Reinking 1978; Greenhut and Gilmer 1985; Ritter, Smith, and Cahoon 1987; Anon. 1991b), the radome method (Larson, Flecher, and Siemers 1980; Brown, Friehe, and Lenschow 1983; Scott et al. 1990; Tjernstrom and Friehe 1991), or a probe-mounted differential pressure flow sensor (Armistead and Webb 1973; Anon. 1991a; Lenschow et al. 1978) for making airflow measurements relative to the aircraft.

In support of the NASA role in global tropospheric research, the Lockheed 188 Electra airplane (designated NASA 429) based at the Wallops Flight Facility was outfitted with a turbulent air motion measurement system (TAMMS). TAMMS utilizes a gust probe with free-rotating vanes affixed to a 3.7-m nose boom and a high-resolution INS used in concert with fast-response chemical instrumentation to make airborne flux measurements of trace species. The latest technology was employed to construct a thick-walled epoxy-graphite composite boom system with a natural frequency that is sufficient to preserve measurements with a 10-Hz bandwidth. The TAMMS has obtained flux measurements of trace species over the Amazon River Basin as well as tundra and wetland regions in North America (Ritter et al. 1990, 1992, and 1994).

The accurate measurement of the three-component ambient wind from an airborne platform is complex and requires an overall calibration of the air motion system. The calibration must cover the entire range of flight conditions encountered during data flight legs. Systematic errors in pressure and temperature measurements are induced by the enhanced kinetic energy and distortion of the airflow local to the aircraft body, which can often contaminate measurements acquired in a flight program. Calibration flights and in-flight maneuvers provide data needed to characterize and compensate for these errors. Errors in the velocity of the aircraft with respect to Earth are dictated by the quality of the inertial navigation system. The discussion and characterization of inertial system errors, however, are not within the scope of this paper. Instead we focus on the characterization and calibration of the gust probe and the overall TAMMS

platform employed for the determination of species flux. The following topics are discussed:

1. Fundamentals of air motion measurement
2. Instrumentation
3. An analysis of the fundamental issues of concern for airborne air motion measurements
4. Flight calibration techniques and validation results

2. Background of Air Motion Measurement

The three-component ambient wind field vector **V**, as related to a local Earth coordinate system, is defined to be

$$\mathbf{V} = \mathbf{i}u + \mathbf{j}v + \mathbf{k}w \tag{1}$$

where u and v are the horizontal wind velocity components and w is the vertical wind velocity component. The unit vectors **i**, **j**, and **k** represent the three-component direction in a right-hand orthogonal coordinate system. The ambient wind field **V** is obtained from an airplane by the vector sum of the air velocity with respect to the airplane ($\mathbf{V}_a$) and the airplane velocity with respect to the Earth ($\mathbf{V}_p$) as expressed by

$$\mathbf{V} = \mathbf{V}_a + \mathbf{V}_p \tag{2}$$

The transformations and actual expressions used to determine the ambient horizontal (u and v) and vertical (w) wind components from airplanes into the standard meteorological frame of reference have been derived and discussed in detail by Axford (1968) and Lenschow (1972). These complex equations, however, can be simplified to the following approximate calculations (Lenschow 1972):

$$u = -U_a \sin(\psi + \beta) + u_p \tag{3a}$$

$$v = -U_a \cos(\psi + \beta) + v_p \tag{3b}$$

$$w = -U_a \sin(\theta - \alpha) + w_p \tag{3c}$$

where

U_a	true airspeed
ψ	airplane heading
β	sideslip angle
θ	pitch angle
α	angle of attack
u_p, v_p, w_p	three-dimensional airplane velocities related to Earth coordinate system (obtained from INS)

A diagram of the coordinate system, airplane attitude angles, and reference axes used to calculate air velocity components is shown in figure 1. Equations (3) identify parameters that make the most significant contributions in the calculation of ambient wind components. These equations can be used to estimate the required accuracy limits of these parameters for making useful air motion measurements. Lenschow (1986) discusses and provides an example of these limits for airplanes flying at 100 m-s^{-1}, which approximates the typical airspeed of the TAMMS platform.

3. Instrumentation

The Lockheed 188 Electra airplane (based at Wallops Flight Facility) shown in figure 2 has been outfitted with TAMMS which consists of three subsystems: (1) a gust probe equipped for fast-response meteorological and flow angle measurements, (2) a high-resolution INS, and (3) a data acquisition system. (See the appendix for airplane specifications.) The fluctuations in the three-component ambient wind field measured by TAMMS are combined with measurements of a species made from fast-response (>10 Hz) chemical instrumentation to make airborne eddy correlation flux measurements. The vertical flux of a species c is given by

$$\bar{F} = \overline{w'c'} \tag{4}$$

where

$$w' = w - \bar{w} \tag{5}$$

$$c' = c - \bar{c} \tag{6}$$

and the bar over the symbol and prime denote the mean value and the fluctuation from the mean value, respectively. Sample periods are typically 10 to 20 min in duration to obtain a statistically significant sampling.

The flight calibration of TAMMS employed the tower flyby method to accurately characterize the impact of airplane motion on the measurement of free-stream static air pressure and static air temperature. This method requires an instrumented tower for correlative static ground measurements. A C-band radar facility complemented the calibration procedure by providing continuous and accurate altitude data during tower flyby maneuvers and additional calibration flight maneuvers performed remotely from the tower. The airplane system and the ground instrumentation associated with the TAMMS flight calibration are discussed in sections 3.1, 3.2, and 3.3.

3.1. Nose Boom and Meteorological Instrumentation

The nose boom is a conical composite structure fabricated from high-modulus graphite preimpregnated with an epoxy resin. It is 3.7 m in length, 25.4 cm in diameter at the base, and 7.6 cm in diameter at the tip. The wall thickness of the cone decreases from 0.61 cm at the base to 0.46 cm at the tip. An NACA research-type combination pitot-static tube is attached to the tip of the graphite boom. This position places the meteorological instruments and airflow sensors as listed in table I at a distance forward of the fuselage which significantly reduces the influence from the airflow around the airplane. Constructing a boom system of sufficient length that will totally remove the influence of airflow about an airplane is not physically possible. Differential and absolute pressure transducers for impact and static pressure measurements, respectively, are housed in the pitot-static tube–boom mounting adapter. Fast-response temperature and humidity sensors are mounted to the adapter. Flow-direction vanes are located on an NACA combination pitot-static and flow-direction probe. The overall instrument configuration is shown in figure 3 and weighs approximately 31 kg. The boom is mounted at the base to a support frame housed within the radome which accommodates the INS. This support frame is rigidly attached through truss structures mounted to the forward fuselage bulkhead. A Honeywell Primus 800 weather radar mounts above the support frame between the truss structures without field-of-view restrictions in the forward or zenith directions. The lowest natural frequency of the overall INS, support structure, and boom system is 15.3 Hz, which is sufficiently beyond the desired 0–10 Hz bandwidth.

The static and differential pressures, which are critical parameters in determining true airspeed U_a, are measured by Paroscientific Digiquartz pressure transducers, models 215-AW-002 and 5006-D-002, respectively. These transducers employ a crystalline-quartz resonator which measures change in pressure via their pressure-dependent oscillation frequency. Busse (1987) provides a detailed explanation of transducer mechanics and operation. Application accuracy of the transducers is cited by the manufacturer to be 0.01 percent of full scale with 1×10^{-8} resolution. Both the differential and absolute pressure transducers are housed in a thermally insulated and thermostatically controlled "cocoon." Thermal stability of the transducers is obtained with Du Pont Kapton laminated etched-foil heating elements controlled with an inhouse feedback circuit. The thermal environment of the pressure transducers is set at a control temperature of $44°\mathrm{C} \pm 0.5°\mathrm{C}$ to maintain temperature stability during normal operating conditions.

Temperature measurements needed to determine U_a are made with a Rosemount model 102 non-deiced total air temperature T_t sensor housing with a fast-response platinum sensing element (E102E4AL) (DeLeo and Werner 1960; Werner, DeLeo, and Rogal 1961; Stickney, Shedlov, and Thompson 1990). The E102E4AL element has a nominal 50-Ω resistance and a 20-ms response time. The Rosemount signal conditioner was replaced with an inhouse signal conditioner designed to have a 0- to 10-V output. Rosemount total temperature sensors normally exhibit a measured temperature T_m of $\approx 0.995 T_t$. The sensor is mounted on the starboard side of the pitot-static tube–boom adapter. A high correlation between the yaw angle and total air temperature T_t measurements observed during in-flight calibration maneuvers indicates a shadowing effect from the pitot-static tube and/or adapter, which is discussed later. Also, due to the support structure for the temperature sensing element, the T_t system actually has a two-term exponential response (Lenschow 1972; McCarthy 1973). A numerical filter was employed to recover the high-frequency signal that is lost because of the presence of the supporting structure for the element (Ritter, Smith, and Cahoon 1987).

Airflow angles are determined from a pair of free-rotating balsa vanes mounted orthogonally to the instrument head as shown in figure 3. The vanes are oriented to measure angle of attack and flank angle, that is, the incidence angles of airflow relative to the airplane in the vertical and horizontal planes, respectively. Sideslip is assumed to be equal to flank angle for small angles of attack. The vane assembly is attached to a shaft which rotates in a hollow strut and flange machined from a solid piece of stainless steel for mounting. A bronze sleeve bearing supports the outboard end of the shaft with a synchro repeater attached to the inboard flange end. A 16-bit synchro-to-digital converter was used to obtain the data. As a result, airflow angles of 0.005° were capable of being resolved. With equation (3c), this flow angle translates into a sensitivity of 1 cm-s^{-1} for the vertical velocity component.

Richardson (1971) discusses the design of the vanes and provides data on the dynamic properties as employed by the TAMMS on the Electra airplane at Wallops. Advantages of free-rotating vanes include the measurement of the airstream angles directly; therefore, the need is alleviated for accurate knowledge of aerodynamic coefficients for data interpretation, and the elimination of acceleration sensitivity by mass-balancing each vane (Lenschow 1971; Richardson 1971). The natural frequency of free-rotating balsa vanes was determined by Richardson to be approximately one-half times the square root of the dynamic pressure measured in pascals, which translates to 25 to 50 Hz throughout the range of

the Electra flight envelope. The lower detectable limit of the length scale for turbulent eddies would then be approximately 4 to 8 m with the assumption of an average airspeed of 100 m-s^{-1}. Spectral analyses of flight data from these vanes support these findings and indicate good response over the 10-Hz bandwidth of interest.

A Lyman-Alpha hygrometer (Buck 1976) is mounted on the boom tip adapter aft of the pitot-static tube and flow angle vanes. A slower response EG&G 137 hygrometer is mounted in a window port on the fuselage and used to normalize the Lyman-Alpha signal.

3.2. Inertial Navigation System

The Litton Model LTN-72RH gyro-stabilized inertial navigation system is employed on the Electra aircraft for TAMMS. This system is the high-precision version of the standard LTN-72 model. The RH model has been primarily developed for scientific applications with stringent requirements such as those needed for scientific air motion measurements. It provides an increased update rate of approximately 24 data frames/s on both a binary and binary-coded decimal (BCD) bus in ARINC 561 format. The position error drift is approximately 0.5 km/hr (personal communication from Charles Robinson of Litton Industries, Inc.). The INS is mounted to the base of the boom within the Electra radome by way of an environmentally controlled housing.

The airplane attitude angles obtained from the INS were electrically fed through a 16-bit synchro-to-digital converter to yield an angular resolution of 0.005°. Equation (3c) indicates that for an airplane speed of 100 m-s^{-1}, the required angular resolution for θ is 0.06° in order to meet a short-term resolution requirement of 1 cm-s^{-1} for the vertical velocity fluctuation. The INS used by the TAMMS platform, therefore, easily meets this requirement. The vertical velocity of the airplane w_p is derived by integrating the vertical acceleration output of the INS and bounding it by the third-order barometric-inertial loop algorithm as suggested by Lenschow (1986).

The long-term accuracy of the horizontal velocities u_p and v_p are dictated by INS drift rate. A thorough discussion of inertial systems and the errors present in the resultant velocity measurements are presented by Broxmeyer (1964) and Kayton and Fried (1969). Lenschow (1972) gives a general discussion on the types and orders of magnitude of errors associated with inertial systems.

3.3. Aircraft Data Acquisition System

The TAMMS data acquisition system consists of three subsystems: (1) signal conditioning and interface electronics, (2) a pulse code modulation (PCM) system, and (3) a data recording and display system. A block diagram of the overall system is shown in figure 4.

Analog, synchro, frequency, and ARINC 561 format data signals received from the TAMMS components are sent, via signal conditioning and interface electronics, to the PCM system which uses a remote multiplexer/demultiplexer unit (RMDU) for processing data. Synchro and analog data are recorded at 16- and 12-bit accuracies, respectively. Selected analog signals are filtered by using 8 pole, 6 zero elliptic low-pass filters. Signal cutoff frequencies varied accordingly with the response characteristics of the respective instrumentation (e.g., EG&G 137 hygrometer, 2 Hz; total air temperature sensor, 5 Hz; vertical velocity and fast-response measurements of chemical species, 10 Hz). Data are recorded at 66 Hz by a dedicated 386 personal computer onto a dual disk drive. The dual drive allows a full data disk to be swapped without loss of data. A flight data recorder is also used as a storage backup. A second 386 personal computer performs system control, data analysis, and display tasks in real time.

4. Analysis

4.1. Static Pressure Error

The flow field in front of an airplane is influenced for a relatively large distance at subsonic speeds. Far upstream from the airplane, where fuselage effects on the streamlines are minimal, the total pressure is the sum of the free-stream static and dynamic pressures,

$$p_t = p + q_c \tag{7}$$

The shape of the fuselage nose, primarily, determines the distance ahead of the airplane that the flow field is altered. Because of the blunt nose of the Electra airplane, the streamlines of the oncoming air must diverge rapidly; thus, differences are created between the measured and free-stream pressures. Total pressure p_t is conserved for any point along the aircraft body for subsonic flight as given by

$$p_t = p' + q_c' \tag{8}$$

where the prime denotes local values. The static pressure error Δp defined as

$$\Delta p = p' - p \tag{9}$$

is substituted into equation (8) to get

$$p_t = p + \Delta p + q_c' \tag{10}$$

Subtracting equation (7) from equation (10) gives

$$q_c' = q_c - \Delta p \tag{11}$$

The magnitude of Δp can be substantial for very blunt fuselages. Wind tunnel tests have previously demonstrated that the magnitude of static pressure error, as a ratio of $\Delta p/q_c$, is influenced by nose shape and distance upstream of the nose (Letko 1947). The presence of the airplane fuselage, therefore, causes an increase in the local static pressure as well as a decrease in the local dynamic pressure. Changes in the local pressure field may also result from airflow distortion induced by the presence of the pitot-static tube. The determination of the overall static pressure error is a requisite and can be determined through flight calibration tests (Gracey 1980; Lenschow 1986; Dommasch, Sherby, and Connolly 1961).

An additional source of error in pitot-static systems arises from resonance in the lines between the pressure port and the pressure transducer (Iberall 1950) and, therefore, is a function of the length and diameter of tubing and air density (Nicholls 1982). In the NASA Electra configuration, the length and diameter of tubing are approximately 0.75 m and 0.25 cm, respectively; thus, the resonant frequency is ensured to be above 10 Hz.

Gracey (1958 and 1980), Etkin (1959), and Dommasch, Sherby, and Connolly (1961) primarily associate changes in airflow, which influences $\Delta p/q_c$, with Mach number, angle of attack, and/or lift coefficient. The Mach number is given as

$$M^2 = \frac{2}{\gamma - 1}\left[\left(\frac{q_c}{p} + 1\right)^{\gamma - 1/\gamma} - 1\right] \tag{12}$$

where q_c and p are, respectively, the dynamic pressure and free-stream static pressure (defined earlier). The ratio of specific heats γ, which has a slight dependence on water vapor (List 1971), is given by

$$\gamma = \gamma_o\left(1 - 0.07129\frac{e}{p}\right) \tag{13}$$

where e is partial vapor pressure and $\gamma_o = 1.4028$ for dry air.

As mentioned, $\Delta p/q_c$ is influenced by the lift coefficient C_L, which is defined as

$$C_L = \frac{L}{q_c S} \tag{14}$$

where L is lift which is equivalent to the weight of airplane for level flight and S is wing area. Because of the difficulty in determining and monitoring aircraft weight during flight, angle of attack is usually correlated with nondimensional position error:

$$\frac{\Delta p}{q_c} = f(\alpha) \tag{15}$$

This correlation is possible because C_L and angle of attack are linearly related for small angles and a given airplane configuration (Gracey 1980); this allows angle of attack to be substituted for C_L in these conditions. Thus, from equation (14) the nondimensional static pressure error at the static port varies with angle of attack. Altering the airplane configuration also affects the flow field and position error. Pressure errors due to acceleration are relatively small and become negligible with flight leg scenarios which are primarily kept at steady conditions and below $M = 0.5$. Consideration of a much wider dynamic range of flight parameters is recognized for the calibration of high performance aircraft and expanded range of flight conditions (Haering 1990; Bjarke and Ehernberger 1989).

4.2. Static Air Temperature

The static air temperature (i.e., the temperature of the static, undisturbed air through which the airplane is traveling) is actually the last of four temperature values that must be determined for any given point. The four temperatures in order of derivation are (1) measured temperature T_m, (2) recovery temperature T_r, (3) total temperature T_t, and (4) static temperature T_s. These parameters are discussed in detail by Stickney, Shedlov, and Thompson (1990). For our purposes a short summary will suffice.

Static air temperature T_s is related to the total temperature T_t by

$$T_t = T_s\left(1 + \frac{\gamma - 1}{2}M_l^2\right) \tag{16}$$

where M_l denotes the local Mach number as determined by local values of static and dynamic pressure. Estimations of the difference in local static and dynamic pressures were made for the Rosemount total temperature probe located 0.6 m downstream from the pressure ports. The increase of the local static pressure at the Rosemount sensor was thus estimated to be approximately 10 percent of the free-stream dynamic pressure.

The recovery temperature T_r is related to T_t by

$$T_t = \frac{T_r}{1 - \eta} \tag{17}$$

where η is the recovery correction given by

$$\eta = \frac{(1-r)[(\gamma-1)/2]M_l^2}{1+[(\gamma-1)/2]M_l^2} \tag{18}$$

where r is the recovery factor for the sensor. The recovery factor is a function of the aerodynamics of the sensor and its location on the aircraft and must therefore be determined experimentally. For each data point as the aircraft passed the tower, r was determined from

$$r = \frac{T_r - T_{s,\mathrm{ref}}}{T_t - T_{s,\mathrm{ref}}} \tag{19}$$

where $T_{s,\mathrm{ref}}$ is the reference static temperature as determined from tower measurements interpolated to aircraft altitude. Finally the measured temperature T_m is related to T_r by

$$T_r = T_m - T_x \tag{20}$$

where T_x is an error due to self-heating effects and is generally negligible. True airspeed, as indicated in equation (3), contributes in the calculation of all wind vector components.

True airspeed U_a is expressed as

$$U_a^2 = \gamma R T_s M^2 \tag{21}$$

where R is gas constant. It is apparent from equations (3), (9), (11), (12), and (21) that the accuracy of air motion measurements is dependent on the accurate determination of T_s and free-stream impact and static pressures. The temperature and pressure measurements used in the calculation of U_a, however, must be determined from measurements that are characteristic of the free-stream or undisturbed air. Since these measurements were obtained from sensors located on the gust probe, they must be corrected for kinetic energy effects and position error due to the disturbance of the airplane body to the free-stream airflow. These corrections for the TAMMS are determined through dedicated in-flight maneuvers and validation tests which are discussed in detail in sections 5 and 6.

5. Flight Calibration Techniques

Techniques employed to calibrate sensors and determine systematic errors encountered by air motion measurement systems are well known and documented (Shrager 1964; DeLeo and Hagen 1966; Anon. 1971; Gracey 1980; DeAnda 1981; and Brown 1985). A variation of the tower flyby method with radar tracking was implemented for the calibration of static pressure position error and T_s for the TAMMS platform. A description of the test setup and procedure is in section 5.1.

In-flight maneuvers performed remotely from the tower are also included in the calibration procedure. These maneuvers modulate var ious airflow configurations relative to the airplane and are required to correct flight measurements and evaluate the overall performance of TAMMS. Procedures call for these maneuvers to be performed for the initial calibration and determination of systematic system errors. The need to account for any changes in flow vane characteristics and ensure data integrity also requires that these maneuvers be performed on a regular basis on data flights. The various in-flight maneuvers utilized for air motion system calibrations are discussed by Axford (1968), Telford and Wagner (1974), Lenschow et al. (1978), and Lenschow (1986). The procedures applied to the overall calibration of TAMMS consist of speed variation, skid, pitch, and reversed heading maneuvers, and are discussed in sections 5.2, 5.3, 6.1, and 6.2.

5.1. Tower Flyby

A 91.5-m tower located at the Wallops Flight Facility was used for flight calibration of the TAMMS platform (fig. 5). A tracking C-band radar located 3483 m from the instrumented tower was used to record precise three-dimensional position data of the Electra airplane during the TAMMS calibration flight. The radar employs an rf amplifier and is designed specifically for precision, long-range tracking. The Electra was outfitted with a transponder for optimal precision tracking. The range and angle precision of the radar is 2.75 m (rms) and 0.05 mils (rms), respectively. This translates to approximately ±0.2 m in aircraft altitude. The radar transmitting and receiving frequency range is 5400 to 5900 MHz with a minimum range of 550 m.

The tower was instrumented to measure absolute pressure, air temperature, and dew point. Air temperature measurements were made by thermistor sensors with an accuracy of ±0.2°C at 91.5 m, 76.2 m, and ground levels. Static air pressure and dew point measurements were made at 91.5 m. The absolute atmospheric pressure sensor consisted of a Paroscientific pressure transducer (0 to 1035 hPa) housed in a thermally controlled enclosure for environmental stability and is identical to the transducer used on the TAMMS platform. (See section 3.) Preceding and following the calibration flight, further correlation between the airplane and tower pressure sensors was obtained by direct comparison to a SONIX digital pressure system developed by Pressure Systems, Inc., to meet calibration standards.

The airplane path was straight, level, unaccelerated, and just below the top of the tower for approximately

30 s before and after passage of the tower. Tower flyby calibration data were taken during 21 passes at 5 different speeds. A clean, aerodynamic profile was maintained (i.e., no flaps) at all times. Passes were made with the flight path offset approximately 2 to 3 wingspans (100 m) from the tower. Data taken on the airplane were averaged at 10 Hz to match the radar sampling rate. Reference values for air temperature $T_{s,ref}$ and pressure $p_{s,ref}$ were determined for comparison with values obtained from the TAMMS platform within 3 s of passage of the tower. These reference values were based on the height data obtained from the radar and the temperature and pressure reference measurements made on the tower. Because pitch attitude changed with airspeed of the airplane during the tower flybys, the reference height (determined from radar tracking) was geometrically corrected for the difference between the vertical position of the radar transponder and static pressure sensor.

Letko (1947) published wind tunnel data indicating the variation of $\Delta p/q_c$ with x/D for a body with a blunt-shaped nose (x is distance of static port in front of nose and D is fuselage diameter). Wind tunnel data shown in figure 6 indicate $\Delta p/q_c$ is constant during level flight for Mach numbers within the Electra flight envelope and x/D ratio (O'Bryan, Danforth, and Johnston 1955). Roe (1951), however, also presents data (fig. 7) that illustrate a slight $\Delta p/q_c$ relationship to angle of attack; thus, tower flyby data for the TAMMS configuration (fig. 8) support a relationship between $\Delta p/q_c$ and angle of attack.

Static pressure error (difference between TAMMS static pressure and free-stream static pressure interpolated from tower to airplane height), obtained from tower flybys, ranged from approximately 3 hPa at Mach number 0.2 to 9 hPa at Mach number 0.45. An approximate value of 0.075 was determined for $\Delta p/q_c$ with a slight correlation to angle of attack as indicated by the tower flyby data shown in figure 8. These results are highly correlative to the wind tunnel data in figures 6 and 7.

Figure 9 shows the experimentally obtained values of the recovery factor for the temperature probe as a function of M_l. These data indicate that although a second-order curve is shown to describe the variation of r with airspeed, a value of 0.98 could be used over the speed range of the airplane with minimal error. Calculated total and static air temperatures as a function of M_l are shown in figure 10. The obvious correlation of airspeed with T_t is not present, as should be expected, for the calculated T_s data curve. The difference between the reference tower temperature and the airborne static temperature measurements for each pass of the tower was determined and indicated no dependence on airspeed. Although no speed dependence is noticeable, the airborne measurements were found to be ≈0.3°C lower than the reference values, which are near measurement accuracies of the instrumentation.

5.2. Speed Variation Maneuver

The speed variation maneuver was the first of several in-flight maneuvers required to correct measurements of flow angles due to the distortion airflow around the airplane. The maneuver consists of flying at a constant heading and altitude while varying airspeed through the speed range of the airplane. This maneuver modulates angle of attack α and pitch angle θ due to the relation of lift to α and airspeed and allows the alpha vane to be directly calibrated to θ, which is obtained from the INS. Because of upwash effects in front of the airplane, a correction or sensitivity factor is found to be 0.75 for α as indicated by the slope of the plot of α versus θ shown in figure 11. The sensitivity of the alpha vane is not only affected by upwash, but a zero offset is also determined to be 1.35° from the same data set. This offset includes any rotational misalignment of the alpha vane synchro repeater caused by the nose boom configuration and installation. This procedure was repeated during missions to compensate for shifts in offset and sensitivity of the flow angle vanes.

These maneuvers are also used to check the dependency of T_s on airspeed. Adiabatic effects on the temperature sensor (i.e., measured temperature) vary with airspeed. The removal of these effects is done through computations which require a known recovery factor for the sensor. Errors in determining this value or the measurement of airspeed show a periodic relationship between T_s and airspeed; this indicates a dependence of T_s on airspeed. The time series plot of T_s and airspeed shown in figure 12, however, indicates no such relationship and reinforces the validity of airspeed and temperature sensor calibrations.

5.3. Skid Maneuver (Yaw or Sideslip)

Airplane heading ψ, horizontal velocity components, and sideslip β are modulated during the skid maneuver while altitude and roll are kept constant. Skid maneuvers are necessary for in-flight calibration of the sensitivity factor and estimation of errors associated with the beta vane. Sensitivity and offset values are unique to each flow vane installation and must be determined accordingly. Sideslip flight calibrations, however, cannot assume that the horizontal winds are negligible in contrast to the calibration of the angle of attack when vertical winds are assumed to be zero. Tjernstrom and Friehe (1991) describe a flight calibration technique employed for sideslip, which assumes for homogeneous low-turbulence conditions that all variations in the computed horizontal wind are induced by the skid maneuver only.

The sensitivity factor determined under homogeneous and low-turbulence conditions during skid maneuvers is assumed to be highly representative of the beta vane. The offset value, which may include a bias error related to ψ from the INS alignment, however, is determined by adjusting the offset value until the cross-track wind component is equivalent in magnitude for both directions of a reversed heading maneuver. Calibration errors associated with the beta vane are indicated by a periodic variation in computed horizontal velocity during skid maneuvers. The beta vane sensitivity factor was found to be 0.81 with an offset of 1.10°. These values rendered horizontal wind field measurements of less than 10 percent of $U_a(\sin \beta)$, which meet the criteria for satisfactory system performance.

Sideslip, similar to angle of attack, influences static pressure measurements. A time series plot of the aircraft sideslip motion, measured static pressure, and corrected static pressure for a skid maneuver is shown in figure 13. The large sinusoidal curve indicates the sideslip angle as measured by the rotating vane. A split scale is used, for data presentation purposes, to offset the measured static pressure (p', upper curve) from the final static pressure values (p, lower curve) which are determined through calibration as a function of β and q_c'.

Data from sideslip maneuvers indicate an asymmetric relationship of sideslip with calculated static air temperature T_s'. A time history plot of sideslip, T_s', and corrected T_s is presented (in similar fashion as the previous static pressure data set) in figure 14. The variation in T_s' was removed for positive sideslip angles by using the corrected static pressure to determine M_l values. This approach, however, was not sufficient to remove the larger variations in T_s' during negative sideslip angles. The nonsymmetrical relation of T_s' with sideslip is attributed to the nose boom configuration (fig. 3), which shows the total temperature probe mounted horizontally on the starboard side of the boom. This position produces a shielding effect during a negative sideslip angle. An empirical multiplication factor was determined and applied to previously determined static pressure corrections to yield local static pressure conditions and subsequently M_l encountered by the total temperature probe during negative sideslip. The resultant T_s with the majority of the asymmetric effects from shielding removed is indicated by the lower curve in figure 14.

6. Flight Validation Maneuvers

6.1. Pitch Maneuver

Vertical airplane velocity, airspeed, and angle of attack are modulated during a pitch maneuver, whereas roll and sideslip are kept constant. The purpose of the pitch maneuver is to indicate any errors in the determination of vertical winds w or, conversely, demonstrate the overall ability of the air motion system to remove vertical airplane motion and make ambient vertical wind measurements. Lenschow (1986) suggests a period of 10 to 20 s for the pitching motion with an airplane vertical velocity of 2.5 to 4 m-s^{-1} for this maneuver. The airplane vertical velocity and ambient vertical wind determined from a pitch maneuver are plotted for comparison in figure 15. The amplitude of airplane vertical velocity oscillation is varied between 6 and 20 m-s^{-1} with a 20- to 30-s period. The general performance criteria for an air motion system are that errors in calculated vertical winds be less than 10 percent of the airplane vertical velocity. These criteria, as illustrated, are easily met during the test conditions.

6.2. Reversed Heading Maneuver

The reversed heading maneuver demonstrates the ability of the air motion system to measure the ambient horizontal wind components u and v by modulating airspeed and sideslip angle errors. From equations (3), ψ, u_p, and v_p are obtained through the INS leaving U_a and β as determined by the pitot-static tube, T_t sensor, and beta vane measurement; thus, the calibrations of these sensors are critical and directly influence horizontal wind measurements.

Reversed headings are performed by flying at a constant altitude and heading for approximately 3 min and then reversing the course in a manner in which the return course passes through the same air mass. These maneuvers are performed above the boundary layer in a homogeneous air mass to ensure the sampling of the same meteorological conditions as realistically possible. A time history plot of along-track winds during a reversed heading maneuver performed along the prevailing wind direction is shown in figure 16(a) and demonstrates the ability of the system to make accurate, true airspeed measurements. A reversed heading is immediately performed adjacent to the first and perpendicular to the prevailing wind. Cross-track winds obtained in these conditions are shown in figure 16(b) and are similar, as expected, to the along-track winds. This similarity indicates that the sum of sideslip and heading has been adequately determined. Horizontal wind, obtained by vector addition of along- and cross-track winds from a previous flight track is shown in figure 16(c).

7. Concluding Remarks

The calibration of a turbulent air motion system from in-flight and tower flyby maneuvers using a tracking C-band radar has been discussed. A description of the gust probe measurement technique and instrument

package, flight calibration procedures, and results were included. The primary goals that have been addressed consist of: (1) defining any dependence of static air temperature to airspeed, (2) determining systematic static pressure position error as related to platform configuration, and (3) demonstrating the overall system consistency to make accurate three-dimensional ambient wind field measurements.

The total air temperature probe recovery factor of 0.98 was determined experimentally through analysis of the tower flyby calibration data. Comparison of airplane-derived static air temperature T_s with tower air temperature data and speed variation maneuvers performed remotely from the tower illustrated the lack of dependence between T_s and airspeed; consequently, the calibration of the air temperature probe was verified. Further flight tests (skid maneuvers), however, indicated a shadowing effect on the total air temperature probe induced by the pitot-static tube mounting configuration on the nose boom. This shadow effect was successfully removed through the application of a numerical filter to the air temperature data.

Calibration data acquired for the determination of static pressure position error of the gust probe were found to closely approximate data obtained from previously documented wind tunnel tests. Analysis of tower and flight data showed a high correlation of position error to impact pressure with a slight dependence on angle of attack and/or lift coefficient C_L. Because of the difficulty in obtaining a reasonable approximation of airplane weight during flight and the linear relationship of angle of attack with C_L for small angles, angle of attack was substituted for C_L. As a result, static pressure error was determined to be defined adequately as a function of impact pressure and angle of attack. Pitch, skid, and reversed heading maneuvers demonstrated the overall ability of the air motion system to remove aircraft motion and make ambient vertical and horizontal wind measurements. The general rule applied to airborne platforms used to make air motion measurements states that the calculated vertical winds should be <10 percent of the platform vertical velocity and calculated horizontal winds should be <10 percent of $U_a(\sin \beta)$ (where U_a is true airspeed and β is sideslip angle). These criteria have been met and provide ample confidence in the system to provide reliable measurements of the ambient three-component wind field during straight and level flight conditions.

NASA Langley Research Center
Hampton, VA 23681-0001
October 4, 1996

Appendix

Specifications of Lockheed 188 Electra Airplane

The Lockheed 188 Electra airplane based at Wallops Flight Facility and designated NASA 429 is a low-wing, medium altitude, moderate range transport airplane powered by four Allison turboprop engines.The specifications of the airplane are given as follows:

Wing:
- Area, m^2. . . . . 120.8
- Span, m 30.2

Fuselage:
- Diameter, m 3.45
- Overall length (excluding boom and pitot-static tube), m. 32.25

Weight:
- Takeoff gross weight, kg 52 730
- Payload capacity, kg 10 450
- Maximum fuel loading, kg 15 450

Performance:
- True airspeed, $m\text{-}s^{-1}$ 90–160
- Flight endurance at 155 $m\text{-}s^{-1}$, hr 5.5
- Maximum operating altitude, km 7
- Cruising altitude, km 4.5–7

Altitude, km	Endurance, hr	Range, km	Airspeed, $m\text{-}s^{-1}$
0.15–3	6	2600	125
3–6	7	2800	125
6–7	7	3100	130

References

Anon. 1971: *Flight Test Procedures for Static Pressure Systems Installed in Subsonic Transport Aircraft*. SAE ARP 921.

Anon. 1991a: Rosemount® Model 858 Flow Angle Sensors. Bul. 1014, Rosemount Inc.

Anon. 1991b: *Wind Measurement*. MRF Instrument Note 10, British R.A.E.

Armistead, Katherine H.; and Webb, Lonnie Dean 1973: *Flight Calibration Tests of a Nose-Boom Mounted Fixed Hemispherical Flow Direction Sensor*. NASA TN D-7461.

Axford, D. N. 1968: On the Accuracy of Wind Measurements Using an Inertial Platform in an Aircraft, and an Example of a Measurement of the Vertical Mesostructure of the Atmosphere. *J. Appl. Meteorol.*, vol. 7, pp. 645–666.

Bjarke, Lisa J.; and Ehernberger, L. J. 1989: *An In-Flight Technique for Wind Measurement in Support of the Space Shuttle Program*. NASA TM-4154.

Brown, E. N.; Friehe, C. A.; and Lenschow, D. H. 1983: The Use of Pressure Fluctuations on the Nose of an Aircraft for Measuring Air Motion. *J. Climat. & Appl. Meteorol.*, vol. 22, pp. 171–180.

Brown, E. N. 1985: *Calibration of the NCAR (National Center for Atmospheric Research) Sabreliner Research Static Pressure Source With a Trailing Cone Assembly*. NCAR/TN-253/EDD.

Broxmeyer, Charles 1964: *Inertial Navigation Systems*. McGraw-Hill Book Co.

Buck, Arden L. 1976: The Variable-Path Lyman-Alpha Hygrometer and Its Operating Characteristics. *Bull. American Meteorol. Soc*., vol. 57, no. 9, pp. 1113–1118.

Busse, Donald W. 1987: Quartz Transducers for Precision Under Pressure. *Mech. Eng.*, vol. 109, no. 5.

DeAnda, Albert G. 1981: *AFFTC Standard Airspeed Calibration Procedures*. AFFTC-71H-68-1001, U.S. Air Force.

DeLeo, Richard V.; and Werner, Frank D. 1960: Temperature Sensing From Aircraft With Immersion Sensors. Preprint No. NY60-91, *Fall Instrument-Automation Conference and Exhibit*, Instr. Soc. America, pp. 91-NY60-1–91-NY60-10.

DeLeo, Richard V.; and Hagen, Floyd W. 1966: *Flight Calibration of Aircraft Static Pressure Systems—Final Report*. SRDS Rep. No. RD-66-3, REC Rep. 76431, FAA.

Dommasch, Daniel O.; Sherby, Sydney S.; and Connolly, Thomas F. 1961: *Airplane Aerodynamics*, Third ed., Pitman Publ. Corp.

Etkin, Bernard 1959: *Dynamics of Flight.* John Wiley & Sons.

Frost, Walter; Paige, Terry S.; and Nelius, Andrew E. 1991: *Guide to Measurement of Winds With Instrumented Aircraft*. NASA CR-188601.

Gilmer, R. O.; McGavin, R. E.; and Reinking, R. F. 1978: A Small Aircraft Gust-Probe System for Studies of Boundary Layer Convection and Transport. *Fourth Symposium on Meteorological Observations and Instrumentation of the American Meteorological Society*, pp. 426–432.

Gracey, William 1958: *Measurement of Static Pressure on Aircraft*. NACA Rep. 1364.

Gracey, William 1980: *Measurement of Aircraft Speed and Altitude*. NASA RP-1046.

Greenhut, G. G.; and Gilmer, R. O. 1985: *Calibration and Accuracy of the NOAA/ERL Gust Probe System and Intercomparison With Other Systems*. NOAA-TM-ERL-ESG-22.

Haering, Edward A., Jr. 1990: *Airdata Calibration of a High-Performance Aircraft for Measuring Atmospheric Wind Profiles*. NASA TM-101714.

Iberall, Arthur S. 1950: Attenuation of Oscillatory Pressures in Instrument Lines. *J. Res. Natl. Bur. Stand.*, vol. 45, no. 1, pp. 85–106.

Kayton, Myron; and Fried, Walter R., eds. 1969: *Avionics Navigation Systems*. John Wiley & Sons.

Larson, Terry J.; Flechner, Stuart G.; and Siemers, Paul M., III 1980: *Wind Tunnel Investigation of an All Flush Orifice Air Data System for a Large Subsonic Aircraft.* NASA TP-1642.

Lemone, Margaret A.; and Pennell, William T. 1980: A Comparison of Turbulence Measurements From Aircraft. *J. Appl. Meteorol*., vol. 19, pp. 1420–1437.

Lenschow, D. H. 1971: Vanes for Sensing Incidence Angles of the Air From an Aircraft. *J. Appl. Meteorol.*, vol. 10, pp. 1339–1343.

Lenschow, D. H. 1972: *The Measurement of Air Velocity and Temperature Using the NCAR Buffalo Aircraft Measuring System*. NCAR-TN/EDD-74.

Lenschow, D. H.; Cullian, C. A.; Friesen, R. B.; and Brown, E. N. 1978: The Status of Air Motion Measurements on NCAR Aircraft. *Fourth Symposium on Meteorological Observations and Instrumentation of the American Meteorological Society*, pp. 433–438.

Lenschow, Donald H., ed. 1986: *Probing the Atmospheric Boundary Layer*. American Meteorol. Soc.

Letko, William 1947: *Investigation of the Fuselage Interference on a Pitot-Static Tube Extending Forward From the Nose of the Fuselage*. NACA TN 1496.

List, Robert J. 1971: *Smithsonian Meteorological Tables*, Smithsonian Inst.

McCarthy, J. 1973: A Method for Correcting Airborne Temperature Data for Sensor Response Time. *J. Appl. Meteorol*., vol. 12, pp. 211–214.

Meissner, Charles W., Jr. 1976: *A Flight Instrumentation System for Acquisition of Atmospheric Turbulence Data*. NASA TN D-8314.

Nicholls, Stephen 1982: An Observational Study of the Mid-Latitude, Marine, Atmospheric Boundary Layer. Ph.D. Diss., Southampton Univ.

O'Bryan, Thomas C.; Danforth, Edward C. B.; and Johnston, J. Ford 1955: *Error in Airspeed Measurement Due to the Static-Pressure Field Ahead of an Airplane at Transonic Speeds*. NACA Rep. 1239.

Richardson, Norman R. 1971: *Dynamic and Static Wind-Tunnel Tests of a Flow-Direction Vane.* NASA TN D-6193.

Ritter, J.; Beck, S.; Hedgepeth, R.; Barrick, J.; and Butler, C. 1987: The Development of an Air Motion Measurement System for NASA's Electra Aircraft. *Sixth Symposium on Meteorological Observations and Instrumentation of the American Meteorological Society*, pp. 140–143.

Ritter, John A.; Smith, G. Louis, and Cahoon, Donald R. 1987: The Use of a Numerical Filter to Correct Airborne Temperature Measurements for the Effects of Sensor Lag. *Sixth Symposium on Meteorological Observations and Instrumentation of the American Meteorological Society*, pp. 261–264.

Ritter, John A.; Barrick, John D. W.; Gregory, Gerald L.; Sachse, Glen W.; Hill, Gerald F.; and Lenschow, Donald H. 1990: Airborne Flux Measurements and Budget Estimates of Trace Species Over the Amazon Basin During the GTE/ABLE 2B Expedition. *J. Geophys. Res*., vol. 95, pp. 16875–16886.

Ritter, John A.; Barrick, John D. W.; Sachse, Glen W.; Gregory, Gerald L.; Woerner, Mary A.; Watson, Catherine E.; Hill, Gerald F.; and Collins, James E., Jr. 1992: Airborne Flux Measurements of Trace Species in an Arctic Boundary Layer. *J. Geophys. Res.*, vol. 97, no. D15, pp. 16601–16625.

Ritter, John A.; Barrick, John D. W.; Watson, Catherine E.; Sachse, Glen W.; Gregory, Gerald L.; Anderson, Bruce E.; Woerner, Mary A.; and Collins, James E., Jr. 1994: Airborne Boundary Layer Flux Measurements of Trace Species Over Canadian Boreal Forest and Northern Wetland Regions. *J. Geophys. Res.*, vol. 99, no. D1, pp. 1671–1685.

Roe, M. 1951: *Position Error Calibration of Three Airspeed Systems on the F-86A Airplane Through the Transonic Speed Range and in Maneuvering Flight.* Rep. No. NA-51-864, North American Aviation, Inc.

Scott, Stan G.; Bui, T. Paul; Chan, K. Roland; and Bowen, Stuart W. 1990: The Meteorological Measurement System on the NASA ER-2 Aircraft. *J. Atmos. & Ocean. Tech*., vol. 7, pp. 525–540.

Shrager, J. J. 1964: *Calibrating Static Pressure Systems at Low Altitudes—Final Report*. RD-64-37, FAA.

Stickney, Truman M.; Shedlov, Marvin W.; and Thompson, Donald I. 1990: *Rosemount Total Temperature Sensors*. Tech. Rep. 5755, Rev. B, Rosemount, Inc.

Telford, J. W.; and Wagner, P. B. 1974: The Measurement of Horizontal Air Motion Near Clouds From Aircraft. *J. Atmos. Sci*., vol. 31, pp. 2066–2080.

Telford, J. W.; Wagner, P. B.; and Vaziri, A. 1977: The Measurement of Air Motion From Aircraft. *J. Appl. Meteorol*., vol. 16, pp. 156–166.

Tjernstrom, Michael; and Friehe, Carl A. 1991: Analysis of a Radome Air-Motion System on a Twin-Jet Aircraft for Boundary-Layer Research. *J. Atmos. & Ocean. Tech.*, vol. 8, pp. 19–40.

Werner, F. D.; DeLeo, R. V.; and Rogal, B. 1961: Total Temperature Probes. *Flight*.

Table I. TAMMS Sensor Characteristics

Parameters	Sensor	Accuracy	Resolution	Response
Dew point	EG&G 137 hygrometer	±0.5°C	0.1°C	2–10 sec
Dew point	AIR-LA-1AC Lyman-Alpha hygrometer	±0.6°C	0.03°C	2 ms
Air temperature	Rosemount model 102 non-deiced series sensor	±0.2°C	0.006°C	[a]2 Hz
Flow angles	Free-rotating balsa vanes (synchro resolver)	±0.2°C	0.005°C	25–50 Hz
Static pressure	Paroscientific Digiquartz absolute pressure transducer	±0.21 hPa	0.052 hPa	1 ms
Differential pressure	Paroscientific Digiquartz differential pressure transducer	±0.083 hPa	0.021 hPa	1 ms
Pressure altitude	Rosemount 1241B capacitive transducer	±0.4 percent (0 to 4.5 km)	1 m at sea level	15 ms

[a]Extended to ≈8 Hz with numerical filter (Ritter et al. 1987).

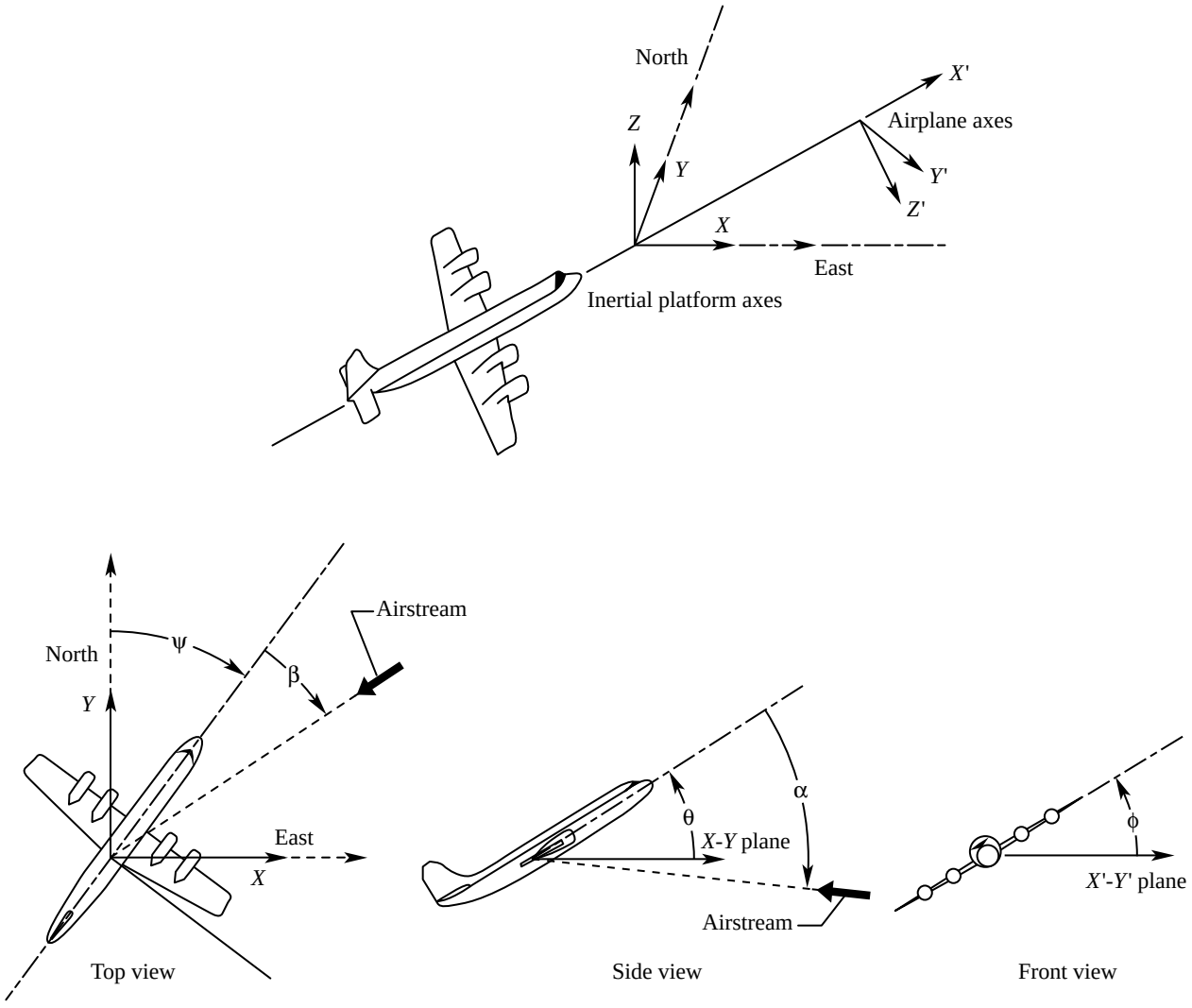

Figure 1. Coordinate system, airplane attitude angles, and reference axes used to calculate air velocity components.

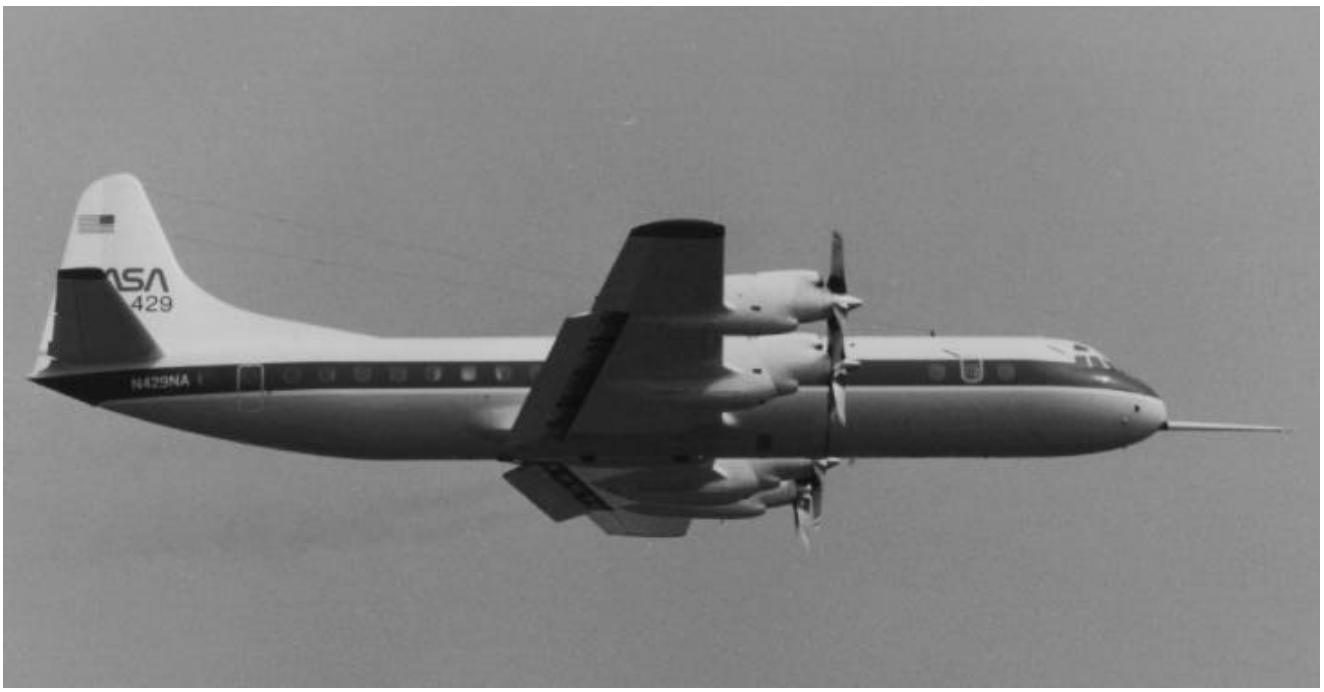

WI-84-368-6

Figure 2. Lockheed 188 Electra airplane (NASA 429) at Wallops Flight Facility.

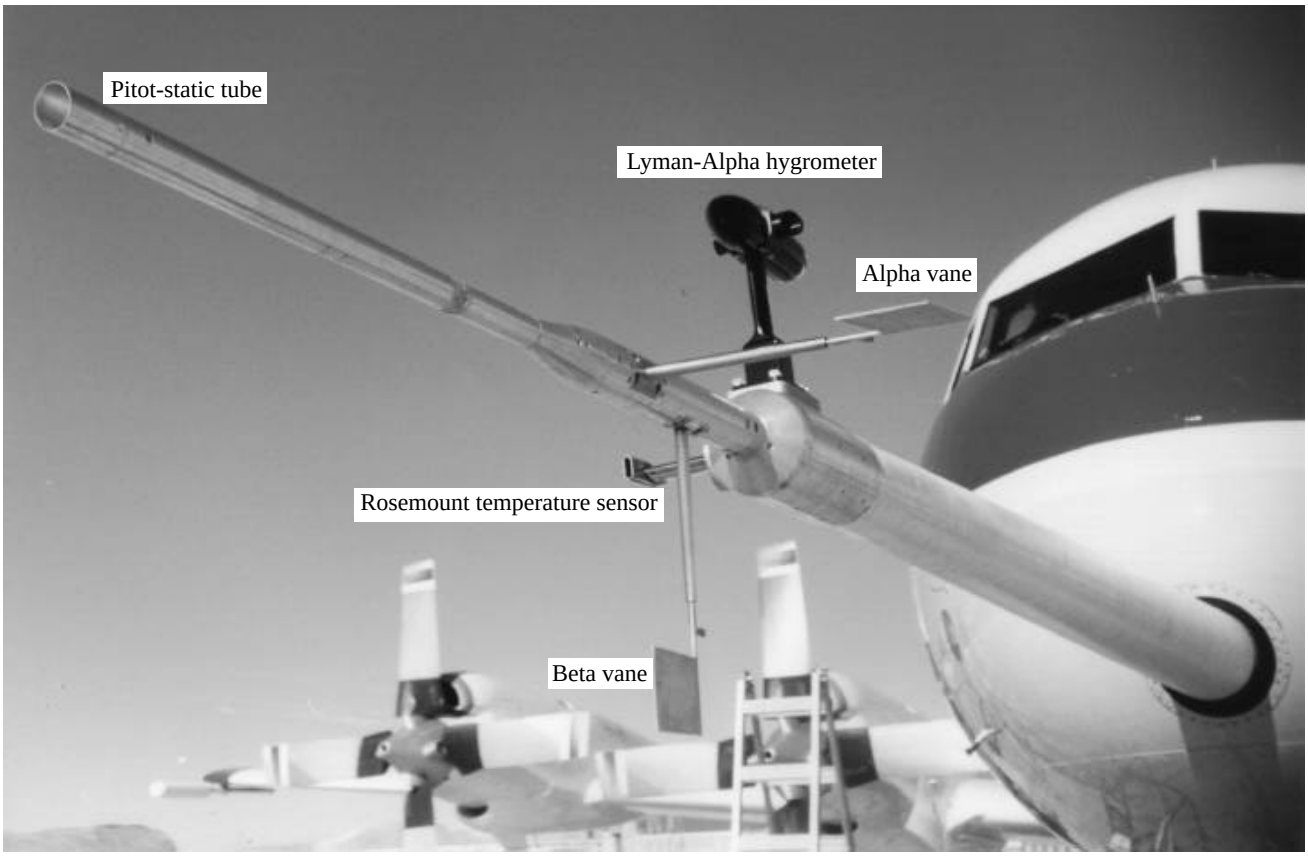

Figure 3. TAMMS gust probe.

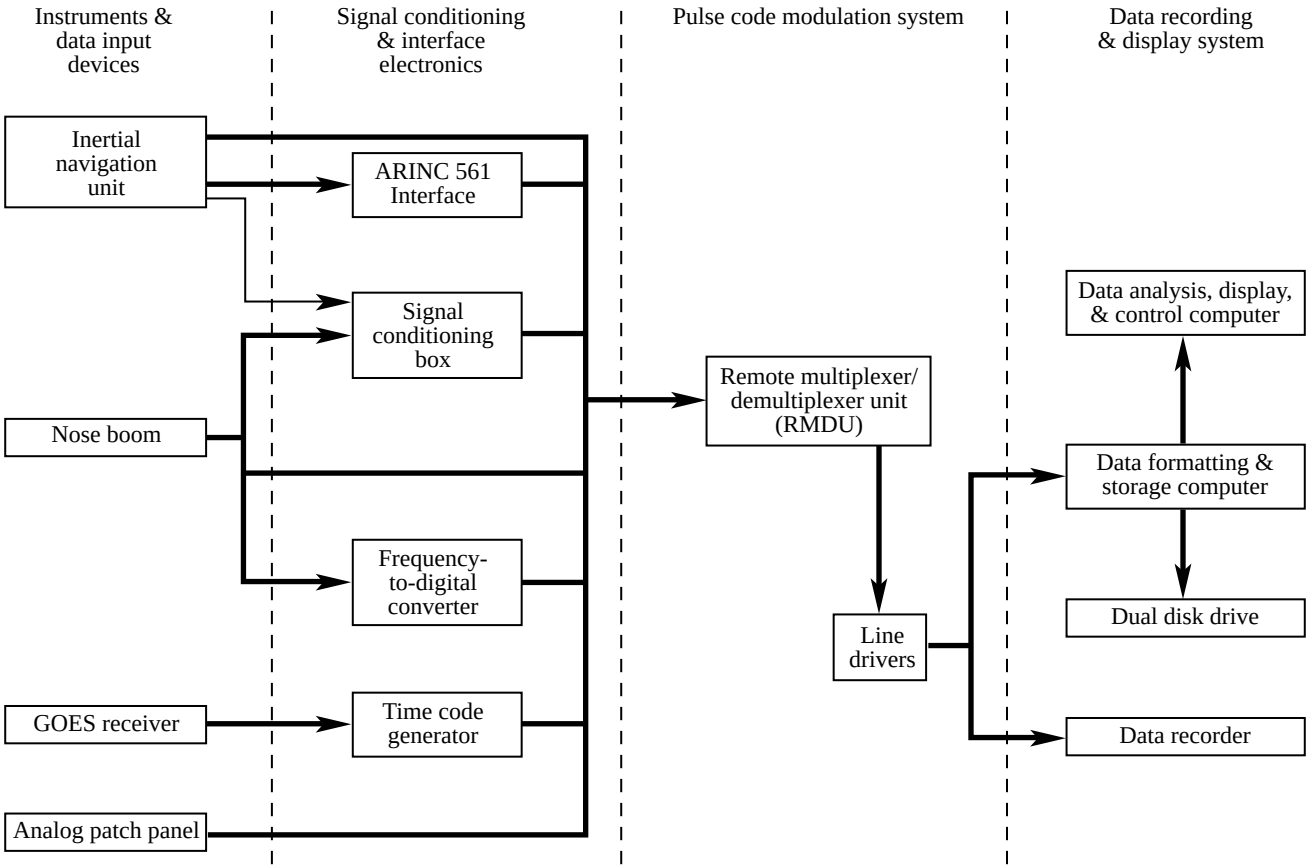

Figure 4. Block diagram of TAMMS data acquisition system.

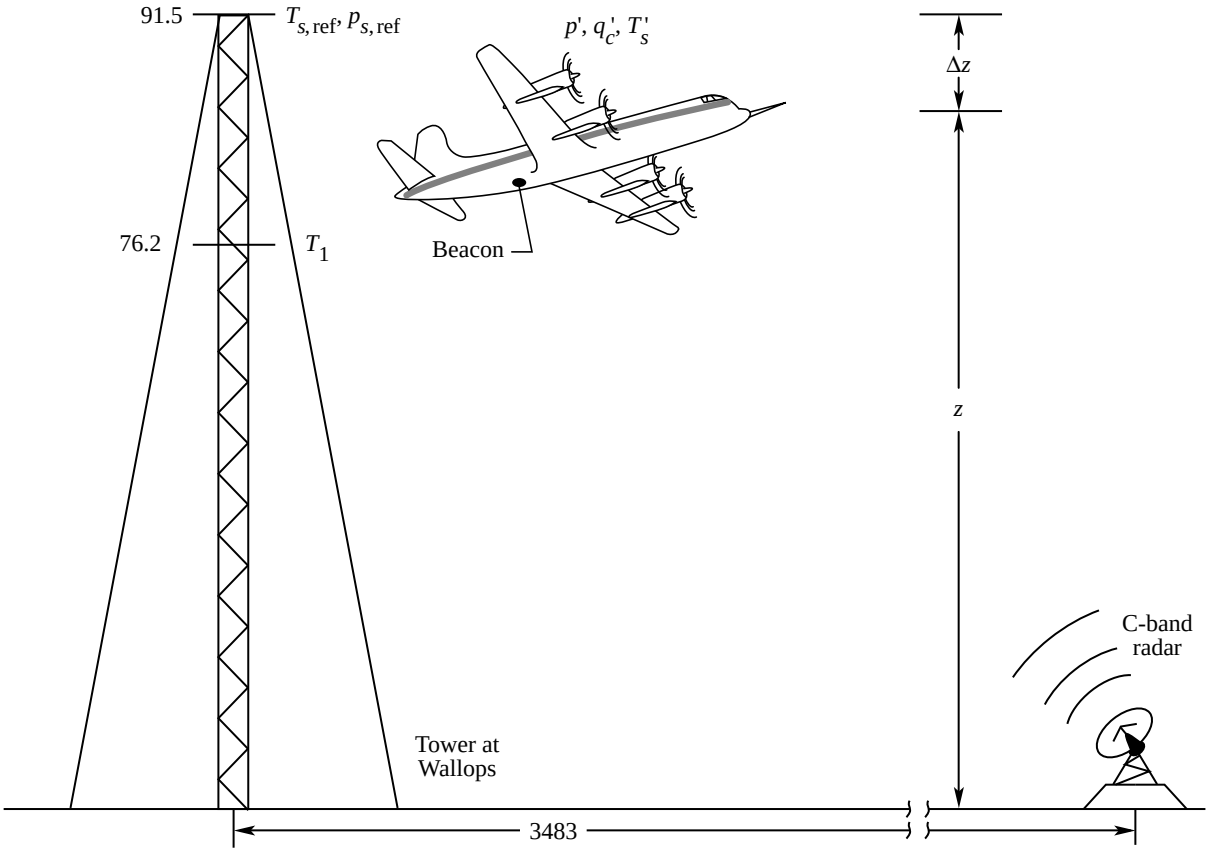

Figure 5. Illustration of tower flyby test setup. Dimensions are in meters.

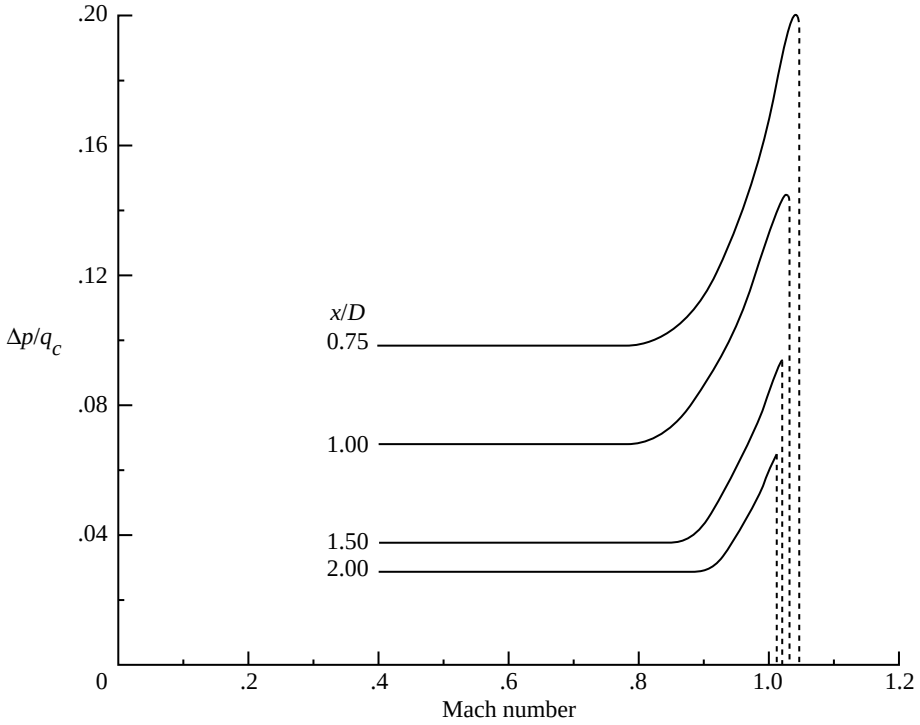

Figure 6. Wind tunnel data illustrating variation of static pressure error as influenced by Mach number at different distances ahead of aircraft fuselage (O'Bryan, Danforth, and Johnston 1955).

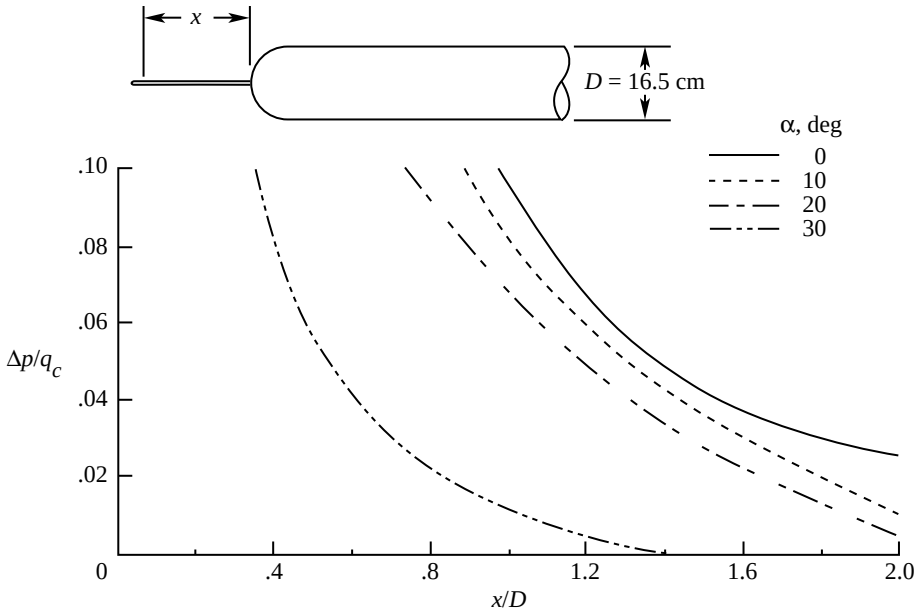

Figure 7. Wind tunnel data showing effect of angle of attack on static pressure error forward of airplane with blunt-shaped nose similar to Electra airplane. (Data from Roe 1951.)

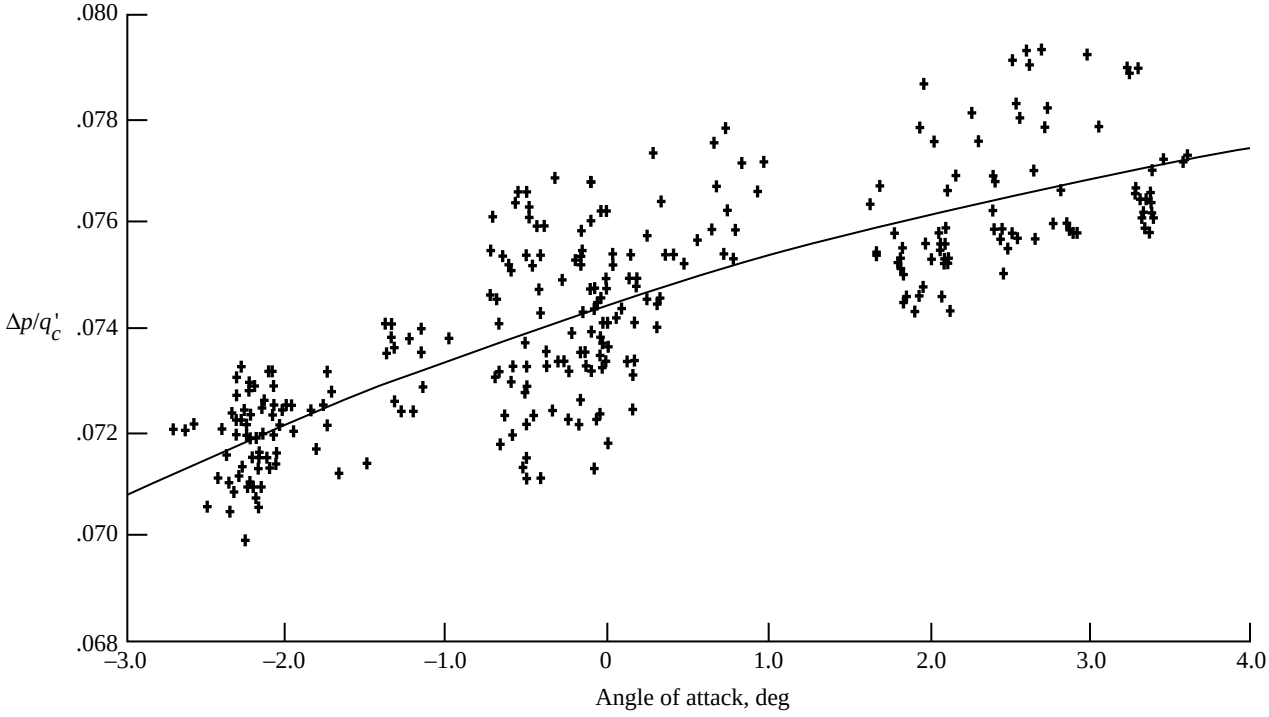

Figure 8. Static pressure error determined from tower flyby test data as function of angle of attack.

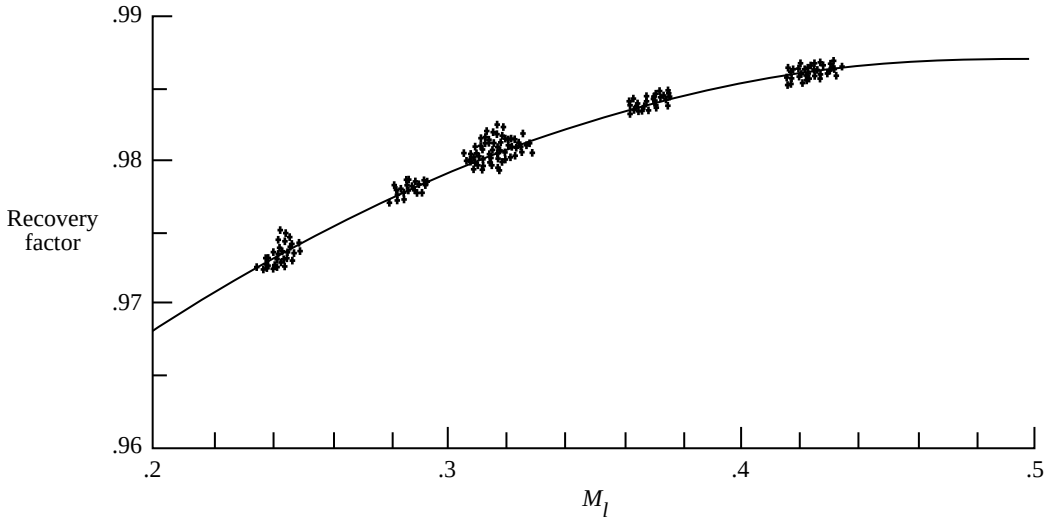

Figure 9. Recovery factor for TAMMS total air temperature probe as function of Mach number.

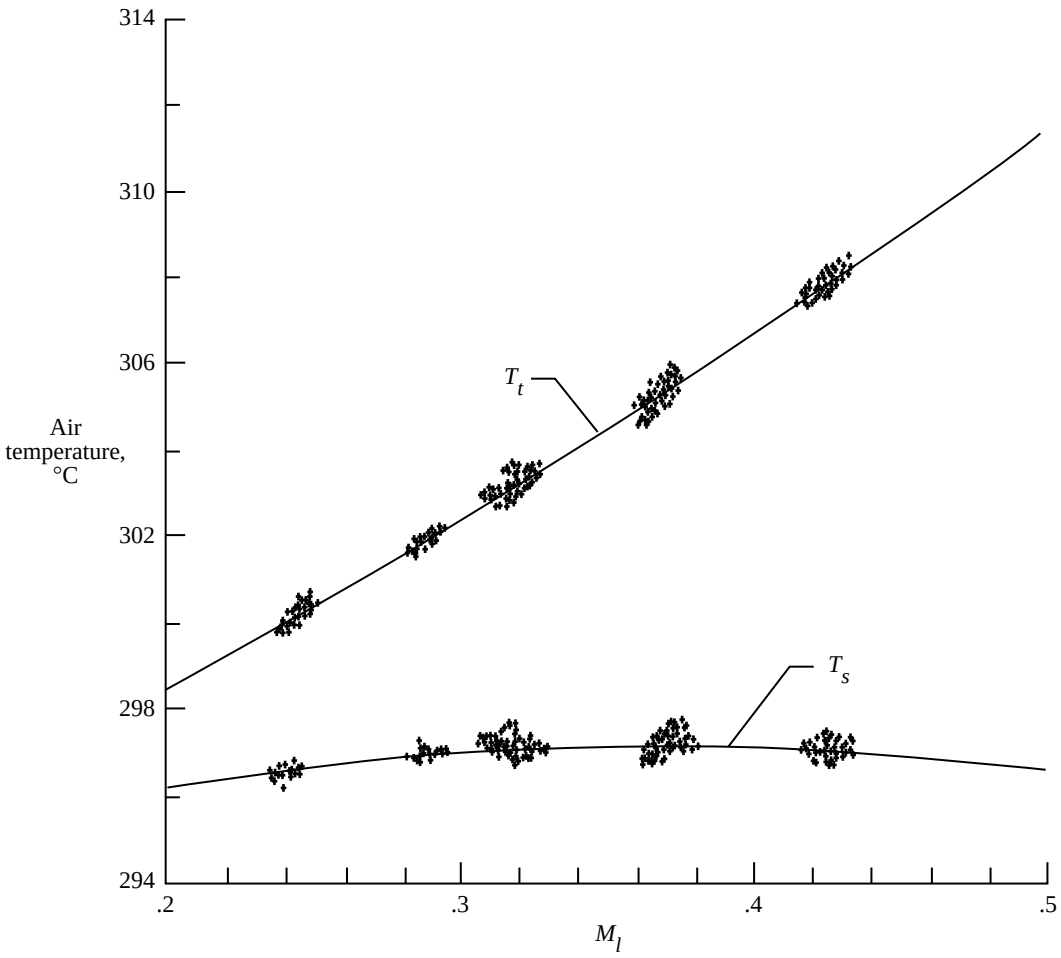

Figure 10. Tower flyby data indicating dependent nature of total air temperature and required isolation of static air temperature on Mach number.

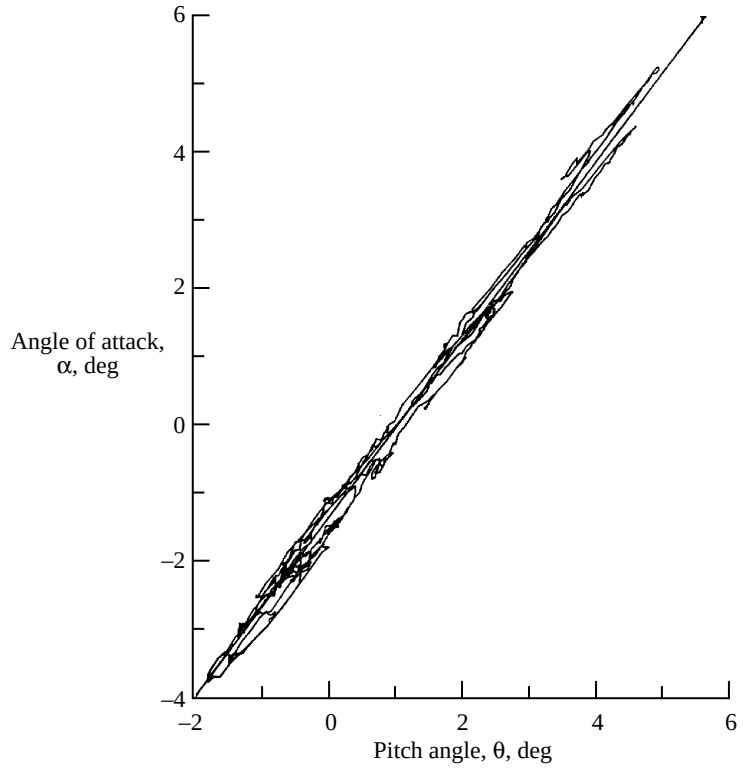

Figure 11. Calibration results for angle of attack vane from speed variation maneuver.

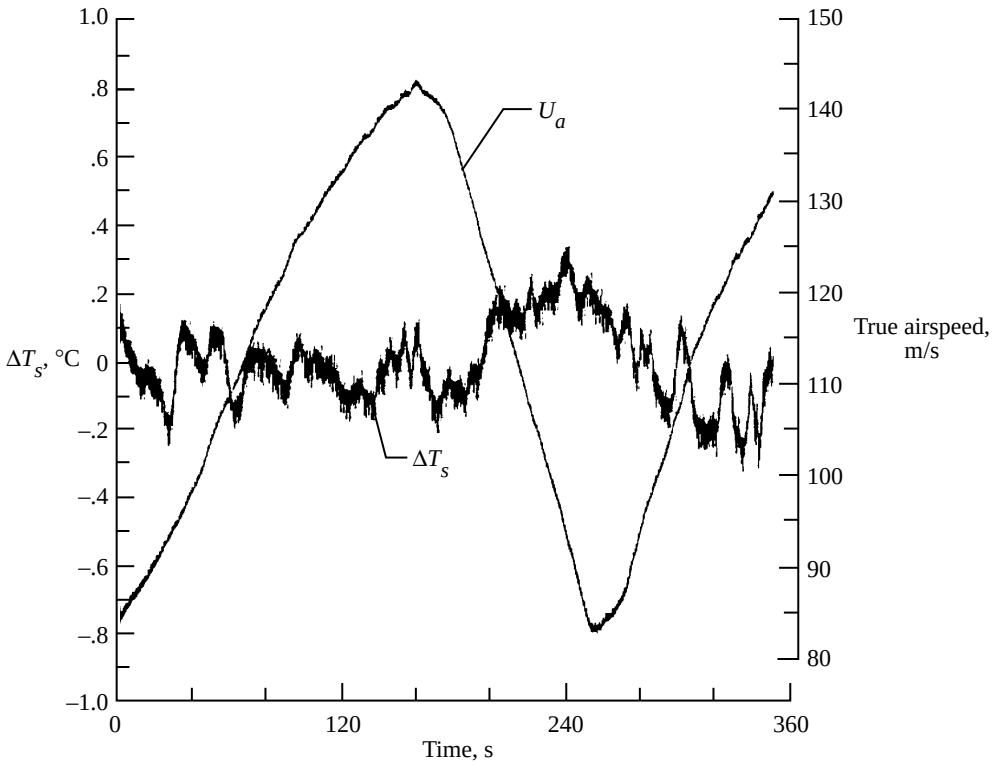

Figure 12. Time series plot of static air temperature during speed variation maneuver.

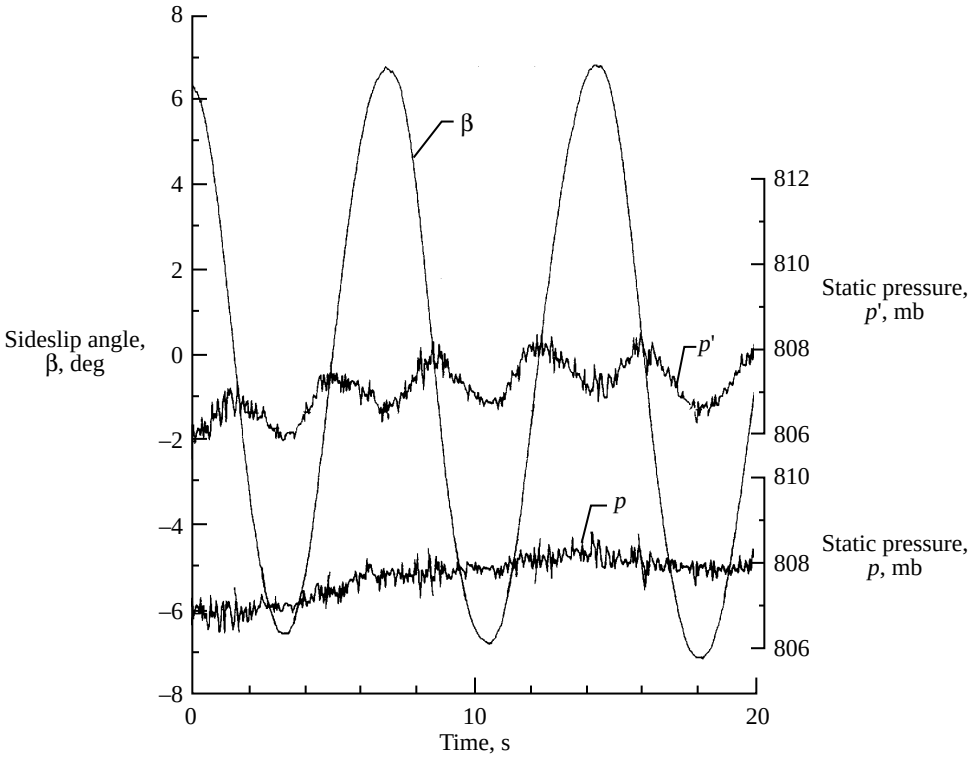

Figure 13. Time series plot of sideslip, measured static pressure p', and corrected static pressure p obtained during skid maneuver.

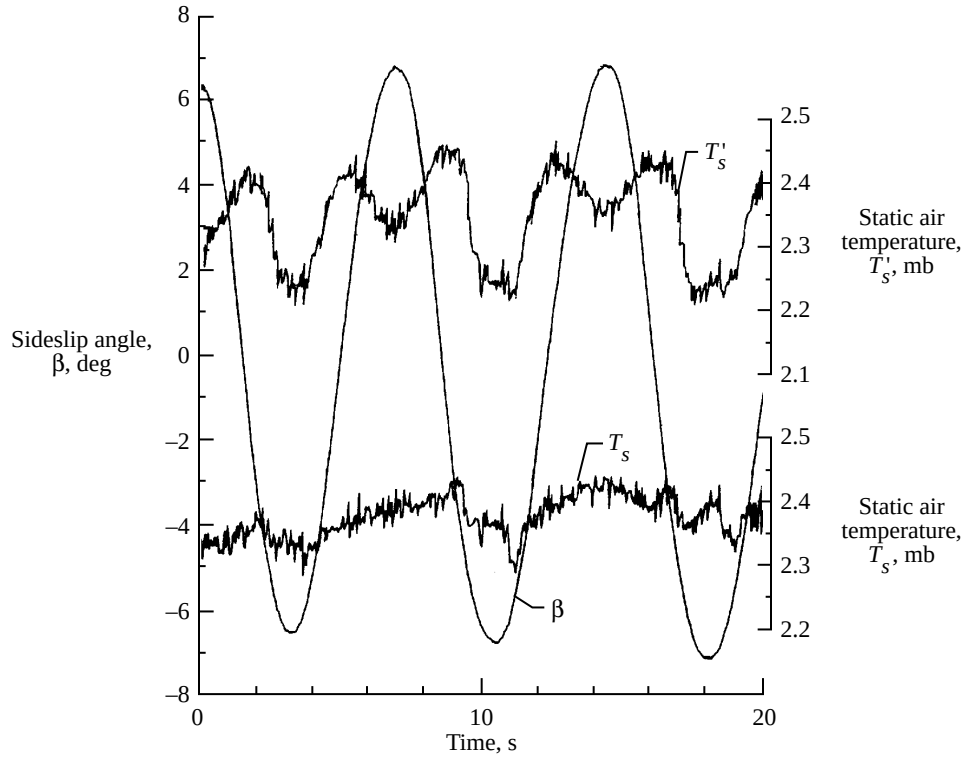

Figure 14. Time series plot of sideslip, calculated static air temperature T_s', and corrected static air temperature T_s obtained during skid maneuver.

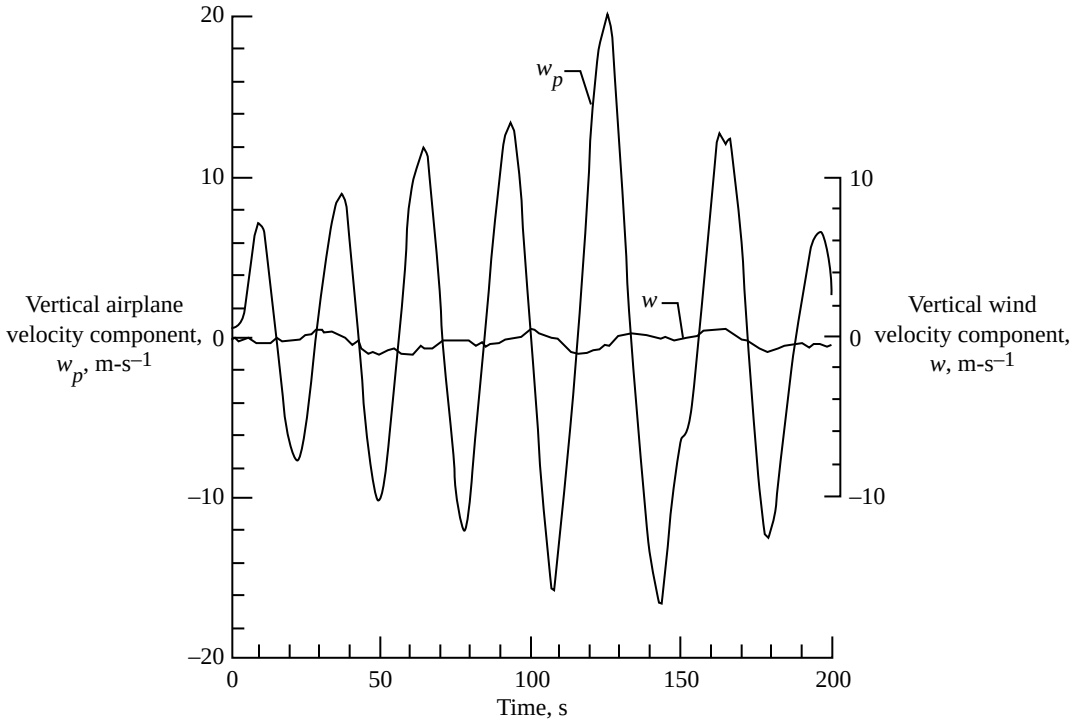

Figure 15. Time series plot of aircraft vertical velocity and vertical wind component as determined by TAMMS during pitch maneuver.

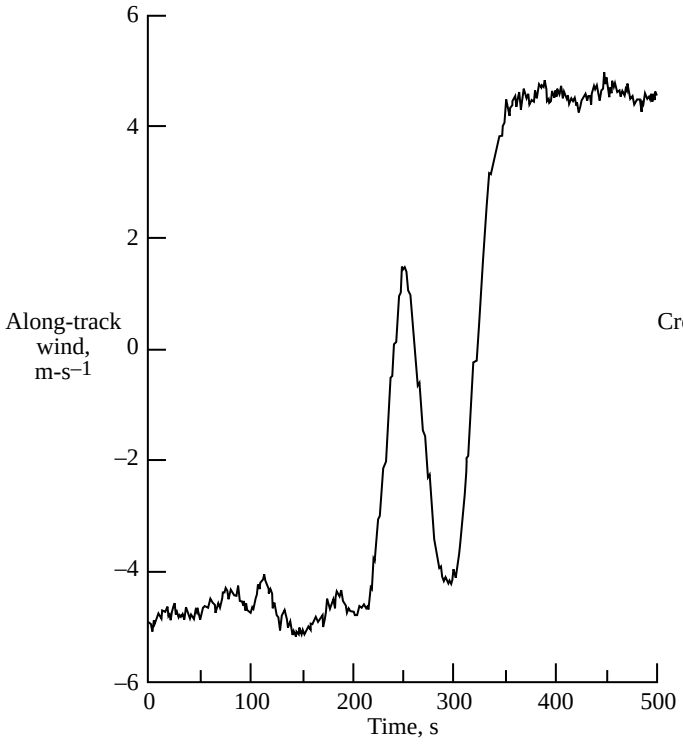

(a) Along-track wind.

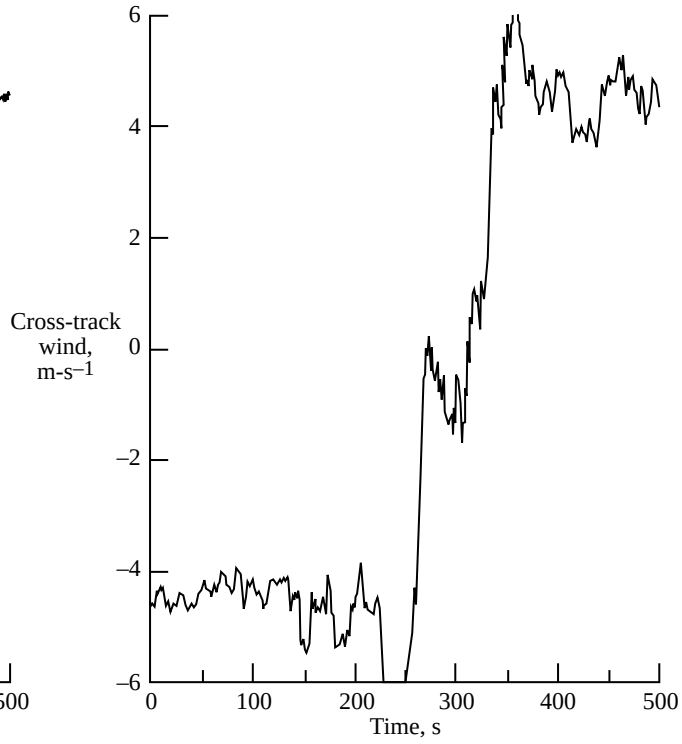

(b) Cross-track wind.

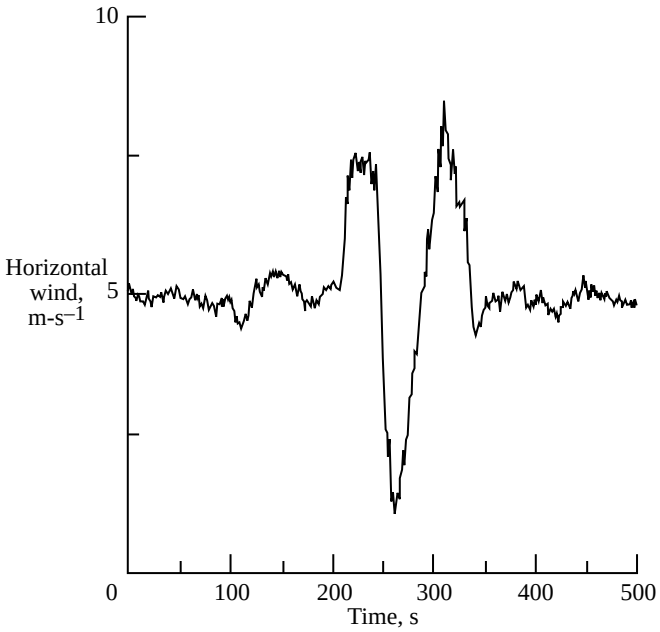

(c) Horizontal wind.

Figure 16. Plots of winds as determined by vector addition.

REPORT DOCUMENTATION PAGE

Form Approved
OMB No. 0704-0188

1. AGENCY USE ONLY *(Leave blank)*	2. REPORT DATE	3. REPORT TYPE AND DATES COVERED
	December 1996	Technical Paper

4. TITLE AND SUBTITLE
Calibration of NASA Turbulent Air Motion Measurement System

5. FUNDING NUMBERS
WU 464-54-13-70

6. AUTHOR(S)
John D. W. Barrick, John A. Ritter, Catherine E. Watson, Mark W. Wynkoop, John K. Quinn, and Daniel R. Norfolk

7. PERFORMING ORGANIZATION NAME(S) AND ADDRESS(ES)
NASA Langley Research Center
Hampton, VA 23681-0001

8. PERFORMING ORGANIZATION REPORT NUMBER
L-17528

9. SPONSORING/MONITORING AGENCY NAME(S) AND ADDRESS(ES)
National Aeronautics and Space Administration
Washington, DC 20546-0001

10. SPONSORING/MONITORING AGENCY REPORT NUMBER
NASA TP-3610

11. SUPPLEMENTARY NOTES

12a. DISTRIBUTION/AVAILABILITY STATEMENT
Unclassified–Unlimited
Subject Category 01
Availability: NASA CASI (301) 621-0390

12b. DISTRIBUTION CODE

13. ABSTRACT *(Maximum 200 words)*
A turbulent air motion measurement system (TAMMS) was integrated onboard the Lockheed 188 Electra airplane (designated NASA 429) based at the Wallops Flight Facility in support of the NASA role in global tropospheric research. The system provides air motion and turbulence measurements from an airborne platform which is capable of sampling tropospheric and planetary boundary-layer conditions. TAMMS consists of a gust probe with free-rotating vanes mounted on a 3.7-m epoxy-graphite composite nose boom, a high-resolution inertial navigation system (INS), and data acquisition system. A variation of the tower flyby method augmented with radar tracking was implemented for the calibration of static pressure position error and air temperature probe. Additional flight calibration maneuvers were performed remote from the tower in homogeneous atmospheric conditions. System hardware and instrumentation are described and the calibration procedures discussed. Calibration and flight results are presented to illustrate the overall ability of the system to determine the three-component ambient wind fields during straight and level flight conditions.

14. SUBJECT TERMS	15. NUMBER OF PAGES
Aircraft air motion measurement; Static pressure position error; Turbulent air motion	29
	16. PRICE CODE: A03

17. SECURITY CLASSIFICATION OF REPORT	18. SECURITY CLASSIFICATION OF THIS PAGE	19. SECURITY CLASSIFICATION OF ABSTRACT	20. LIMITATION OF ABSTRACT
Unclassified	Unclassified	Unclassified	